

# Studying the Sources of Cosmic Reionization with 21-cm Fluctuations

Rennan Barkana<sup>1,2,3\*</sup>

<sup>1</sup> *Institute for Cosmic Ray Research, University of Tokyo, Kashiwa 277-8582, Japan*

<sup>2</sup> *Division of Physics, Mathematics and Astronomy, California Institute of Technology, Mail Code 130-33, Pasadena, CA 91125, USA*

<sup>3</sup> *Guggenheim Fellow; on sabbatical leave from the School of Physics and Astronomy, Tel Aviv University, Israel*

27 November 2021

## ABSTRACT

We explore the ability of measurements of the 21-cm power spectrum during reionization to enable the simultaneous reconstruction of the reionization history and the properties of the ionizing sources. For various sets of simulated 21-cm observations, we perform maximum likelihood fits in order to constrain the reionization and galaxy formation histories. We employ a flexible six-parameter model that parametrizes the uncertainties in the properties of high-redshift galaxies. The computational speed needed is attained through the use of an analytical model that is in reasonable agreement with numerical simulations of reionization. We find that one-year observations with the MWA should measure the cosmic ionized fraction to  $\sim 1\%$  accuracy at the very end of reionization, and a few percent accuracy around the mid-point of reionization. The mean halo mass of the ionizing sources should be measurable to 10% accuracy when reionization is 2/3 of the way through, and to 20% accuracy throughout the central stage of reionization, if this mass is anywhere in the range 1/3 to 100 billion solar masses.

**Key words:** galaxies:high-redshift – cosmology:theory – galaxies:formation

## 1 INTRODUCTION

The earliest generations of galaxies are thought to have heated and reionized the universe. Ly $\alpha$  absorption shows that the IGM has been a hot plasma at least since  $z \sim 6.5$  (Fan et al. 2006), while the five-year WMAP measurements of the large-angle polarization of the cosmic microwave background imply that the universe was significantly ionized within the redshift range  $z \sim 8$ –14 (Dunkley et al. 2008). The same WMAP measurements are also consistent with the  $\Lambda$ CDM model and, together with distance measurements from supernovae and baryon acoustic oscillations from galaxy surveys, have helped to determine rather accurately the standard cosmological parameters of this model (Komatsu et al. 2008); we thus assume the  $\Lambda$ CDM model with density parameters  $\Omega_m = 0.28$  (dark matter plus baryons),  $\Omega_\Lambda = 0.72$  (cosmological constant), and  $\Omega_b = 0.046$  (baryons), together with  $h = 0.7$  (dimensionless Hubble constant),  $n = 0.96$  (power spectrum index), and  $\sigma_8 = 0.82$  (power spectrum normalization).

Observational study of reionization promises to teach us a great deal about the early generations of galaxies that formed when the universe was between  $\sim 300$  and 800 Myr

in age. An important feature of reionization is that it indirectly probes whatever are the dominant sources of ionizing radiation, even if these are otherwise unobservable; e.g., the universe may have been ionized by large numbers of very small galaxies that are too faint to be detected individually (or even by unexpected sources such as miniquasars or decaying dark matter). The overall timing of reionization versus redshift mainly constrains the overall cosmic efficiency of ionizing photon production. In comparison, a detailed picture of reionization as it happens can teach us a great deal about the sources that produced this cosmic phase transition, particularly in the case of the most natural source, stars in galaxies.

A key point is that the spatial distribution of ionized bubbles is determined by clustered groups of galaxies and not by individual galaxies. At such early times galaxies were strongly clustered even on rather large scales (tens of comoving Mpc), and these scales therefore dominate the structure of reionization (Barkana & Loeb 2004). Overdense regions fully reionize first because the number of ionizing sources in these regions is increased very strongly (Barkana & Loeb 2004). The large-scale topology of reionization is therefore inside out, with underdense voids reionizing only at the very end of reionization, with the help of extra ionizing photons coming in from their surroundings. This picture has

\* E-mail: barkana@wise.tau.ac.il

been confirmed and quantified more precisely in detailed analytical models that account for large-scale variations in the abundance of galaxies (Furlanetto et al. 2004), and in a number of large-scale numerical simulations of reionization (e.g., Zahn et al. 2007; Iliev et al. 2008; Santos et al. 2008).

Cosmic reionization represents an extreme challenge for numerical simulations, because of the enormous range of spatial scales involved (Barkana & Loeb 2004). On the one hand, individual galaxies as small as a comoving kpc may contribute to the early stages of reionization, while ionizing photons may travel as much as 100 Mpc before being absorbed, near the end of reionization (or earlier if X-rays make a significant contribution). Even smaller scales must be resolved in order to probe the dense gas clumps that likely determine the ionizing mean free path and the recombination rate, while star formation and stellar feedback are still further out of reach. While simulations are improving and may soon include hydrodynamics (in addition to the current N-body plus radiative transfer codes), some have tried to bridge the gap of scales by developing fast semi-numerical methods that make substantial use of approximate analytical models (Zahn et al. 2007; Mesinger & Furlanetto 2007).

The most promising probe of the cosmic reionization history is to use new low-frequency radio telescope arrays to detect emission in the redshifted 21-cm line corresponding to the hyperfine transition of atomic hydrogen. 21-cm cosmology is potentially also a great source of fundamental cosmological information, especially if observations reach small scales and high redshifts. The 21-cm fluctuations can in principle be measured down to the smallest scales where the baryon pressure suppresses gas fluctuations, while the cosmic microwave background (CMB) anisotropies are damped on much larger scales (through Silk damping and the finite width of the surface of last scattering). Since the 21-cm technique is also three-dimensional (while the CMB yields a single sky map), there is a much larger potential number of independent modes probed by the 21-cm signal, which could help to detect primordial non-Gaussianity and test inflation (Loeb & Zaldarriaga 2004). However, ionization fluctuations dominate the 21-cm fluctuations during the epoch of reionization, and thus the first generation of 21-cm experiments are expected to bring new discoveries related to the reionization history rather than the fundamental cosmological parameters (e.g., McQuinn et al. 2006). Furthermore, since the observational noise will be too large to produce 21-cm maps, the fluctuations must be measured statistically, and the power spectrum is both the most natural and the highest signal-to-noise statistic. Upcoming experiments include the Murchison Widefield Array (MWA)<sup>1</sup> and the Low Frequency Array (LOFAR)<sup>2</sup>.

While theorists and numerical simulators have begun to elucidate the relation between the properties of the ionizing sources and the 21-cm power spectrum, a key question has not been addressed thus far: assuming the upcoming observations measure the 21-cm power spectrum as expected, how is the power spectrum to be inverted into a determination of the properties of the sources? Such an inversion problem is usually solved by a maximum likelihood (or  $\chi^2$ ) proce-

dure whereby a model is fit to the observed power spectrum in order to determine the best-fit parameters and their uncertainties. In order to explore maximum likelihood fitting of simulated observations, a flexible model is needed that can quickly yield the 21-cm power spectrum predicted for given parameters of the ionizing galaxies. It is important to have a flexible model that does not presume that we can theoretically predict the properties of the ionizing galaxies, which depend on many complex feedback processes. This “reionize-fast” code would essentially play the same role that CMBFAST (Seljak & Zaldarriaga 1996) did for analyses of measurements of the CMB angular power spectrum. Ultimately, this type of code will most likely be developed from an analytical model that includes as much of the detailed physics as possible and is also partly tuned to fit more accurately the results of numerical simulations, analogous to the way that the formula of Sheth & Tormen (1999) for the halo mass function was developed from the original model of Press & Schechter (1974).

In this paper we employ the model from Barkana (2007) in which we solved for the correlated two-point distribution of density and ionization based on the one-point model of Furlanetto et al. (2004). This is currently the most realistic fully analytical model of the 21-cm power spectrum. In the next section we briefly review the model before comparing its predictions to 21-cm power spectra from several numerical simulations of reionization. In the following section we use the model to summarize which galaxy parameters affect the 21-cm power spectrum, and then calculate the expected uncertainties from maximum likelihood fits to simulated sets of observed power spectra.

## 2 THE MODEL: SETUP AND TESTS

### 2.1 The analytical model

Analytical approaches to galaxy formation and reionization are based on the mathematical problem of random walks with barriers. The basic approach is that of Bond et al. (1991), who rederived and extended the halo formation model of Press & Schechter (1974). The idea is to consider the smoothed density in a region around a fixed point in space. We begin by averaging over a large (comoving) scale  $R$ , or, equivalently, by including only small comoving wavenumbers  $k$ . We then lower  $R$ , generating a random walk as power on smaller scales (higher  $k$  values) is added, until we find the first (i.e., largest) scale for which the averaged overdensity is high enough to reach a particular milestone. The needed overdensity is termed the barrier, and the goal is then to find the distribution of points at which the random walk first crosses the barrier. For the halo mass function, spherical collapse yields a constant barrier (i.e., the required initial overdensity, linearly extrapolated to the present, is independent of halo mass or scale  $R$ ).

Furlanetto et al. (2004) showed that the condition of having enough ionizing sources to fully ionize a region corresponds approximately to a linear barrier, and then used the statistics of a random walk with a linear barrier to predict the H II bubble size distribution during the reionization epoch. In Barkana (2007) we found an accurate analytical solution for the corresponding two-point problem

<sup>1</sup> <http://www.haystack.mit.edu/ast/arrays/mwa/>

<sup>2</sup> <http://www.lofar.org/>

of two correlated random walks with linear barriers, using the two-step approximation which Scannapieco & Barkana (2002) had applied to the two-point constant barrier problem. Finding the joint probability distribution of the density and ionization state of two points allows the calculation of the 21-cm correlation function or power spectrum (Barkana 2007).

Following Furlanetto et al. (2004), the appropriate barrier for reionization is found by setting the ionized fraction in a region  $\zeta F_{\text{coll}}$  equal to unity, where  $F_{\text{coll}}$  is the collapse fraction (i.e., the gas fraction in galactic halos) and  $\zeta$  is the overall efficiency factor, which is the number of ionizing photons that escape from galactic halos per hydrogen atom (or ion) contained in these halos. This simple version of the model remains approximately valid even with recombinations if the effective  $\zeta$  is divided by one plus the number of recombinations per hydrogen atom in the IGM, assuming this factor is roughly uniform. In order to find  $F_{\text{coll}}$ , a good starting point is the formula of Sheth & Tormen (1999), which accurately fits the cosmic mean halo abundance in simulations. However, an exact analytical generalization is not known for the biased  $F_{\text{coll}}$  in regions of various mean density fluctuation  $\delta$ .

Barkana & Loeb (2004) suggested a hybrid prescription that adjusts the abundance in various regions based on the extended Press-Schechter formula (Bond et al. 1991), and showed that it fits a broad range of simulation results. In general, we denote by  $f(\delta_c(z), S) dS$  the mass fraction contained at  $z$  within halos with mass in the range corresponding to variance  $S$  to  $S+dS$ , where  $\delta_c(z)$  is the critical density for halo collapse at  $z$ . Then the biased mass function in a region of size  $R$  (corresponding to density variance  $S_R$ ) and mean density fluctuation  $\delta$  is (Barkana & Loeb 2004)

$$f_{\text{bias}}(\delta_c(z), \delta, R, S) = \frac{f_{\text{ST}}(\delta_c(z), S)}{f_{\text{PS}}(\delta_c(z), S)} f_{\text{PS}}(\delta_c(z) - \delta, S - S_R), \quad (1)$$

where  $f_{\text{PS}}$  and  $f_{\text{ST}}$  are, respectively, the Press-Schechter and Sheth-Tormen halo mass functions. The value of  $F_{\text{coll}}(\delta_c(z), \delta, R, S)$  is the integral of  $f_{\text{bias}}$  over  $S$ , from 0 up to the value  $S_{\text{min}}$  that corresponds to the minimum halo mass  $M_{\text{min}}$  or circular velocity  $V_c = \sqrt{GM_{\text{min}}/R_{\text{vir}}}$  (where  $R_{\text{vir}}$  is the virial radius of a halo of mass  $M_{\text{min}}$  at  $z$ ). We then numerically find the value of  $\delta$  that gives  $\zeta F_{\text{coll}} = 1$  at  $S = 0$  and its derivative with respect to  $S$ , yielding the linear approximation to the barrier:  $\delta(S) \approx \nu + \mu S$ . Note that Barkana (2007) and Barkana & Loeb (2008) used an approximation in which effectively each factor on the right-hand side of equation (1) was integrated separately over  $S$ , yielding a simple analytical formula for the effective linear barrier. Here we solve numerically for the barrier using the exact formulas (though the difference in the final results is small).

By the reionization epoch, there are expected to be sufficient radiation backgrounds of X-rays and of Ly $\alpha$  photons so that the cosmic gas has been heated to well above the cosmic microwave background temperature and the 21-cm level occupations have come into equilibrium with the gas temperature (Madau et al. 1997). In this case, the observed 21-cm brightness temperature relative to the CMB is independent of the spin temperature and, for our assumed cosmological parameters, is given by (Madau et al. 1997)

$$T_b = \tilde{T}_b(z) \Psi; \quad \tilde{T}_b(z) = 25 \sqrt{\frac{1+z}{8}} \text{ mK}, \quad (2)$$

with  $\Psi = x^n [1 + D(z)\delta]$ , where  $x^n$  is the neutral hydrogen fraction and the linear overdensity at  $z$  is the growth factor  $D(z)$  times  $\delta$  (which is the density linearly extrapolated to redshift 0). Under these conditions, the 21-cm power spectrum is thus  $P_{21} = \tilde{T}_b^2 P_\Psi$ , and thus a model of the relation between the density and the ionization is all that is needed for calculating the 21-cm power spectrum.

The analytical model thus consists of the following: For a given efficiency  $\zeta$  and minimum halo circular velocity  $V_c$  at redshift  $z$ , find the corresponding linear barrier coefficients  $\nu$  and  $\mu$ , calculate the 21-cm correlation function as a function of separation  $d$  (where at each  $d$  we numerically integrate equation (49) of Barkana (2007)), and then Fourier transform to find the power spectrum at the desired values of  $k$ . Even with the analytical model, this procedure is too slow to apply directly in the  $\chi^2$  fitting, but the power spectrum can be interpolated from a large precomputed table as a function of the three variables  $\zeta$ ,  $V_c$ , and  $z$ . Note that our assumption of a fixed  $\zeta$  (at a given  $z$ ) for all halos above the minimum  $V_c$  is not as strong a restriction as it may appear. Since the halo mass function declines rapidly with mass at the high redshifts of the reionization era, once  $V_c$  is fixed, most of the ionizing sources are close in mass (i.e., within a factor of a few) to the minimum mass. Thus, even if in the real universe  $\zeta$  varies with mass at a given redshift, it is unlikely that the total ionized volume will receive large contributions from a wide range of halo masses.

With the basic setup just described, we are free to apply any values of  $\zeta$  and  $V_c$  at various redshifts where the power spectrum can be observed. The simplest model we use is thus a two-parameter model where  $\zeta$  and  $V_c$  are both assumed to be constant with redshift. However, complex, time-variable feedbacks are likely to be operating during reionization, such as X-ray and UV photo-heating, supernovae and stellar winds, metal enrichment (and the consequent changes in gas cooling and stellar populations), feedback from mini-quasars, and radiative feedbacks that affect  $H_2$  formation and destruction. Many of these feedbacks involve scales that are far too small for direct numerical simulation, certainly within a cosmological context, so instead of trying to use particular models we prefer to parametrize our ignorance using additional free parameters. The third parameter that we add is a coefficient that gives  $V_c$  a linear dependence on  $z$ , and the fourth allows a linear redshift-dependence in  $\zeta$ . Similarly, a fifth and sixth parameter allow a quadratic redshift-dependence in  $\zeta$  and  $V_c$ , thus permitting these parameters to vary more flexibly with redshift (including a slope that may even change in sign during reionization). Our main goal is to see whether the 21-cm power spectrum can help determine both the reionization history and key properties of the ionizing sources, even if we allow for such flexible models of the ionizing sources with six free parameters that are not restricted based on specific models of feedback.

## 2.2 Comparison with numerical simulations

Numerical simulations of reionization are a rapidly developing field. Current simulations are based on purely gravitational N-body codes that are used to locate and weigh

forming halos as a function of time. Radiative transfer codes are then used to find the reionization topology due to ionizing photons coming from the source halos. Thus, simulations offer the potential advantages of fully realistic source halo distributions and accurate radiative transfer. Resources, though, are still stretched when attempts are made to resolve the smallest source halos while having sufficiently large boxes for tracking ionizing photons with the longest mean free paths. Also, while prospects are good for also including hydrodynamics, it seems that astrophysics for the foreseeable future must be included schematically, as in an analytical model. The important aspects of astrophysics that are inserted by hand include at least the star formation rate within each halo, properties of the stellar populations, supernova feedback (including suppression of star formation, metal enrichment, and dust formation), photo-heating feedback, and the escape of ionizing photons from each galaxy.

Since the analytical model we use is limited in using spherical statistics as a simple approximation for radiative transfer, it is useful to compare it to results of numerical simulations. We compare our 21-cm power spectrum predictions based on Barkana (2007) to those measured in numerical simulations of Zahn et al. (2007)<sup>3</sup>, Iliev et al. (2008) and Santos et al. (2008) in Figures 1, 2 and 3, respectively. For comparison, the figures also show the shape of the 21-cm power spectrum if it arose purely from density fluctuations; the normalization of these curves corresponds to a uniformly ionizing universe (see also the next subsection). The figures show the brightness temperature fluctuation

$$\Delta_{21}(k) \equiv \tilde{T}_b(z) \sqrt{k^3 P(k)/(2\pi^2)}. \quad (3)$$

The simulations are all in reasonable agreement with the analytical model. The agreement is especially good with Zahn et al. (2007), where the typical error in  $\Delta_{21}$  is  $\sim 10\%$  although it ranges up to  $\sim 25\%$ . The agreement with Iliev et al. (2008) is good at  $z = 12$ , when density fluctuations are completely dominant, but later during reionization a 25% difference is typical, with the simulation curves showing a somewhat different shape that includes a decrease with  $k$  at  $k \gtrsim 1 h/\text{Mpc}$ . There is good agreement (typically  $\sim 10\%$ ) with Santos et al. (2008) at  $z = 10$ , but at the lower redshift in Figure 3 the simulated  $\Delta_{21}$  is flat over a wider range of  $k$  than the theoretical one is, and they typically differ by  $\sim 30\%$ .

In the comparison, in order to try to match the assumptions in the simulations as closely as possible, in the first two comparisons we assumed in the model that the ionizing emission rate from each halo is proportional to its mass. In test #3, we instead assumed that the emission rate is proportional to the gas infall rate into each halo; this is a more natural assumption within the context of the analytical model, and we use it in all of our model calculations below. In any case, the difference between these two assumptions has a minor effect on the 21-cm power spectrum (for a

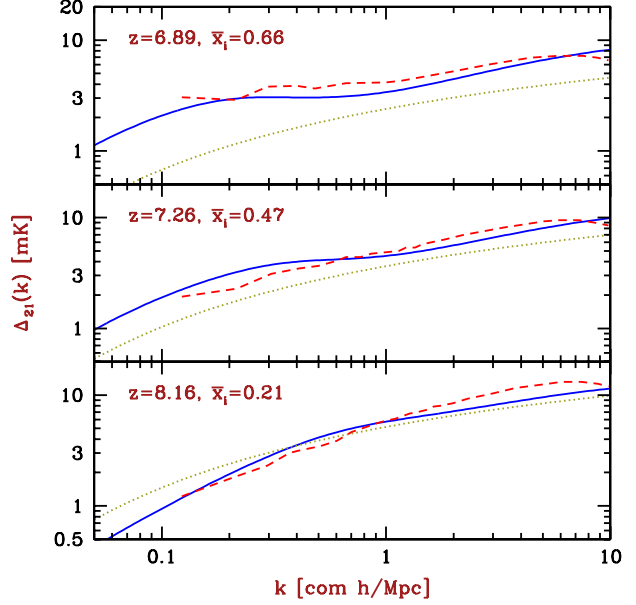


**Figure 1.** The analytical model: Test #1. We compare our predictions for the 21-cm power spectrum using the Barkana (2007) model (solid curves) to those from the simulation of Zahn et al. (2007) (dashed curves). The results are shown at several different redshifts, as indicated in each panel. At each redshift  $z$  we adjust the value of the efficiency in our model in order to match the cosmic mean mass-weighted ionized fraction  $\bar{x}^i$  from the simulation. Also shown (dotted curve) is the 21-cm power spectrum for a uniformly ionized universe at the same  $\bar{x}^i$ .

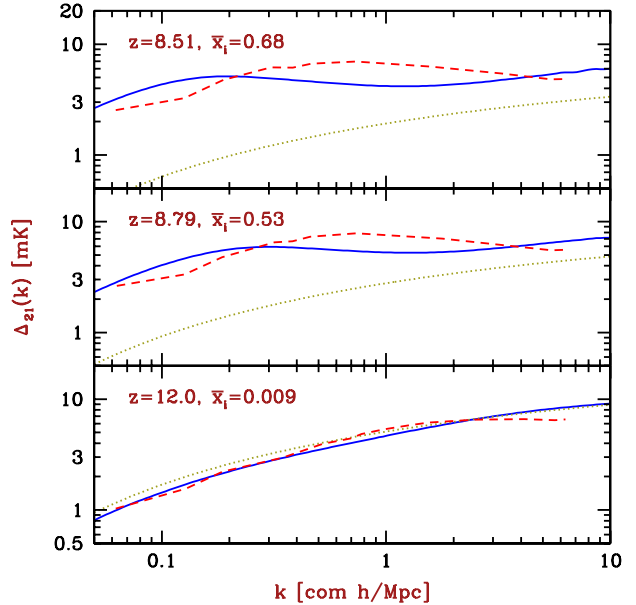


**Figure 2.** The analytical model: Test #2. Same as Figure 1 except that we compare with  $P(k)$  from the simulation f250 of Iliev et al. (2008).

<sup>3</sup> Note that a comparison to these simulations was also shown in Figure 4 of Barkana (2007), but there a preprint of Zahn et al. (2007) was used for results which changed in the final published version, and also there the mass-weighted ionized fraction from the model was incorrectly matched to the volume-weighted one from the simulation.

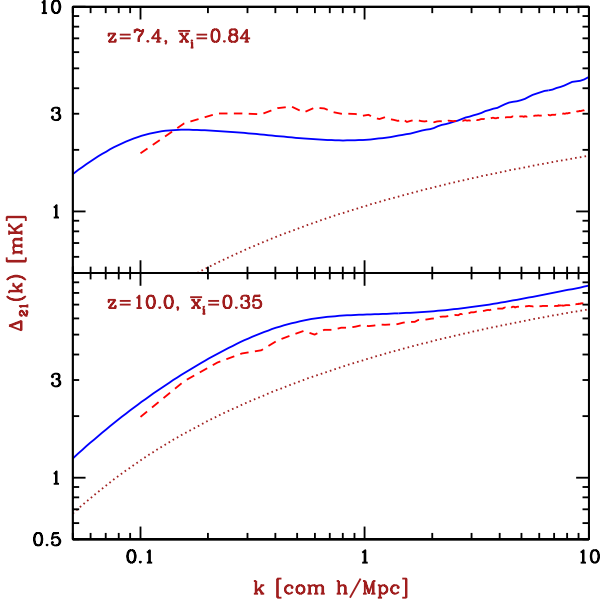


**Figure 3.** The analytical model: Test #3. Same as Figure 1 except that we compare with  $P(k)$  from the simulation of Santos et al. (2008).

fixed value of  $\bar{x}^i$ ). We note that while the analytical model accounts for the restriction of  $x^i$  to a value of 0 or 1, and includes a complex dependence of  $x^i$  on  $\delta$ , it neglects the non-linear growth of  $\delta$ . The latter becomes important only on smaller scales than those accessible to the first-generation 21-cm experiments. For example,  $k \sim 1 h/\text{Mpc}$  corresponds to a scale  $R \sim 9$  comoving Mpc, which at redshift 8 has a root-mean-square fluctuation of 0.14 (on an observed angular scale of  $3'$ ). Also, the model does not include the small gas fraction in leftover neutral clumps within the ionized bubbles, which is important towards the end of reionization. The simulations do include some of the leftover neutral gas, but the limited resolution limits the ability to accurately track these small-scale, non-linear clumps.

From these comparisons we can conclude that the analytical model generally captures the evolution of the 21-cm power spectrum during reionization as seen in the simulations. It is difficult to make a more quantitative assessment, since the varying results in the comparison to the different simulations suggest that the simulations may still disagree among themselves. For further progress, these simulations must be demonstrated to have numerically converged both individually and collectively. Individual convergence would mean showing for each simulation code that the 21-cm power spectrum (over the relevant scales) is independent of the simulated box size (the current sizes produce some large-scale fluctuations in  $\Delta_{21}$  that are obvious in the figures), the N-body resolution (which affects halo formation and structure), and the radiative grid resolution. Collective convergence would mean showing that the various radiative transfer codes all yield the same power spectrum when assuming the same initial conditions and halo astrophysics.

Once numerical convergence is demonstrated, it will become possible to run a suite of simulations in order to test the analytical model more precisely, and perhaps to develop

an improved analytical model based on fitting the numerical simulation results. Such a model can then be used in place of the analytical model that we use here, in order to make more accurate predictions of the 21-cm power spectrum and eventually to fit the real 21-cm data.

### 3 RESULTS

#### 3.1 Parameter dependence

In order to understand what can be learned from observing the 21-cm power spectrum, a key question is which variables mainly determine the 21-cm power spectrum during the reionization epoch. This question has been studied in many papers both analytically and from simulations, in particular by McQuinn et al. (2007) and Lidz et al. (2008). In this subsection we use the Barkana (2007) model to briefly illustrate the expected power spectrum evolution for various assumptions regarding the ionizing source galaxies.

We first note some general properties of the model (see also Furlanetto et al. (2004)). If the universe were uniformly ionized, then we would have  $P_\Psi = (\bar{x}^n)^2 P_\delta$ , where  $\bar{x}^n$  is the neutral hydrogen fraction. Fortunately for the observers, as shown in Figures 1 through 3, the power spectrum is significantly higher in the standard picture where reionization is caused by stellar radiation, resulting in a swiss-cheese division of the IGM into ionized bubbles and neutral regions. In the model we use, on small scales (i.e., much smaller than the H II bubbles),  $P_\Psi \approx \bar{x}^n P_\delta$ , different from the uniformly ionized case since the average value  $\langle (x^n)^2 \rangle = \langle x^n \rangle$  when  $x^n$  can only take on the values 0 and 1. On large scales, if we assume linear fluctuations where the ionized sources have a mean (Lagrangian) bias of  $b > 0$ , so that the ionized fraction fluctuations are  $\delta_{x^i} = b\delta$ , then  $P_\Psi = [1 - \bar{x}^i(1+b)]^2 P_\delta$ . In regions of high density, there are potentially more hydrogen atoms but the neutral fraction is lower, giving rise to an anticorrelation between density and 21-cm emission when  $\bar{x}^i > 1/(1+b)$ . This transition typically occurs early in reionization ( $\bar{x}^i \sim 0.1 - 0.15$ ) if  $b \sim 5 - 10$  for the ionizing sources.

Thus,  $P_{21} \propto P_\delta$  on both large and small scales within the model, but with different normalizations. A transition between these two regimes occurs on scales of order the bubble size, where the power spectrum is often rather flat (in terms of  $k^3 P_{21}(k)$  varying slowly with  $k$ ). Early on, when  $\bar{x}^i \ll 1$ ,  $P_\Psi \approx P_\delta$  on all scales. As reionization proceeds, the bias of the ionizing sources raises the large-scale 21-cm power spectrum, with the characteristic bubble (and transition) scale growing with time. Near the end of reionization, the large-scale regime becomes irrelevant (as the bubble size diverges within the model), and the entire power spectrum drops as most of the hydrogen is ionized and no longer contributes to 21-cm emission.

Figure 4 illustrates the evolution of the 21-cm power spectrum in a model with a constant (i.e., redshift-independent) minimum  $V_c = 35$  km/s for galactic halos, and a constant efficiency set to put the end-stages of reionization (i.e.,  $\bar{x}^i = 98\%$ ) at  $z = 6.5$ . The Figure shows the predicted power spectrum at  $\bar{x}^i = 10\%$  ( $z = 10.5$ ),  $30\%$  ( $z = 8.7$ ),  $50\%$  ( $z = 7.8$ ),  $70\%$  ( $z = 7.1$ ),  $90\%$  ( $z = 6.7$ ), and  $98\%$  ( $z = 6.5$ ). We express the result in terms of the

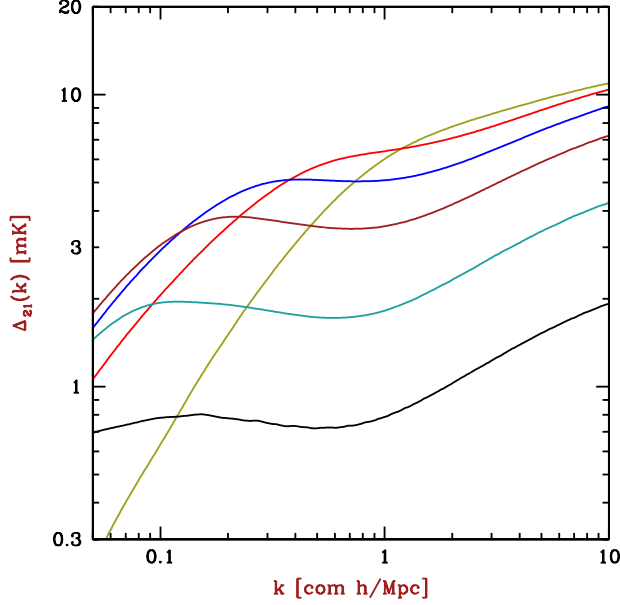


**Figure 4.** Evolution of 21-cm power spectrum throughout reionization, for a model that sets  $\bar{x}^i = 98\%$  at  $z = 6.5$  with minimum  $V_c = 35$  km/s. We consider  $\bar{x}^i = 10\%, 30\%, 50\%, 70\%, 90\%$ , and  $98\%$  (from top to bottom at large  $k$ ).

fluctuation level in units of brightness temperature [eq. (3)]. We note that for this model with  $V_c = 35$  km/s, the overall efficiency is  $\zeta = 31$ , and at the midpoint of reionization ( $\bar{x}^i = 50\%$ ) the minimum galactic halo mass is  $1 \times 10^9 M_\odot$  while the mean halo mass (weighted by ionization intensity) is  $3 \times 10^9 M_\odot$ .

Figure 5 shows the same but with  $V_c = 100$  km/s, i.e., a minimum halo mass higher by a factor of 23. In this case, the same six values of  $\bar{x}^i$  correspond to redshifts  $z = 9.0, 7.8, 7.3, 6.9, 6.6$ , and  $6.5$ . In this model the required efficiency is  $\zeta = 195$ , and at the midpoint of reionization ( $\bar{x}^i = 50\%$ ) the minimum galactic halo mass is  $3 \times 10^{10} M_\odot$  while the mean halo mass (weighted by ionization intensity) is  $5 \times 10^{10} M_\odot$ .

Comparing Figures 4 and 5 we note that in both cases the power spectrum evolution is broadly similar when considered at the same values of  $\bar{x}^i$ , yet there are important differences that allow the power spectrum measurements to probe the characteristic halo mass of the ionizing sources. In particular, more massive halos are more highly biased, and thus produce a higher small- $k$  “bump” during the central stages of reionization. In addition, since more massive halos are more rare and correspond to the Gaussian tail of large (positive) density fluctuations, their abundance changes rapidly with time as density fluctuations grow, thus making reionization more rapid in the case of more massive source halos. In particular, the full period shown in the figures covers the redshift range of  $z = 6.5 - 10.5$  with  $V_c = 35$  km/s but only  $z = 6.5 - 9.0$  with  $V_c = 100$  km/s. Thus, the mass of source halos determines both the height of the large-scale power spectrum and the redshift spread of reionization, and independent measurements of both of these can provide an important consistency check (though see section 4 for additional possible complications that are not included in the model used here).

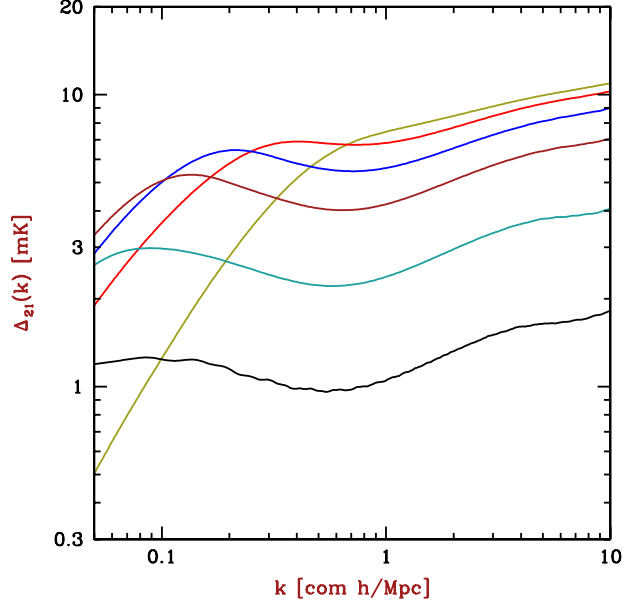


**Figure 5.** Same as Figure 4 except we set  $V_c = 100$  km/s.

For quantitative results, these theoretical predictions must be compared to the expected range and sensitivity of 21-cm power spectrum measurements. We adopt as a specific example of a first-generation experiment the MWA, using a simple fit to the detailed sensitivity analysis of Lidz et al. (2008). Assuming their “super-core” configuration in which the MWA antennae are all packed close together, we find that their results for the measurement noise  $N$  in  $\Delta_{21}$  as a function of  $k$  and  $z$  can be fit as:

$$\log_{10} \left( \frac{N}{2.7 \text{ mK}} \right) \approx 2.8x + 1.1x^2 + (5 + 2.2x) \log_{10} \left( \frac{1+z}{9} \right), \quad (4)$$

where  $x \equiv \log_{10}(k/(h/\text{Mpc}))$ . Over the range  $z = 6.8 - 11.5$  considered in Lidz et al. (2008), this fit is accurate to within a factor of 1.2 in  $N$  for  $k = 0.1 - 0.2 h/\text{Mpc}$  and a factor of 1.4 for  $k = 0.2 - 1 h/\text{Mpc}$ , and corresponds to their observational parameters of a bandwidth of 6 MHz at each redshift (i.e., a  $\Delta z = 0.3$  at  $z = 8$ ),  $k$  bins of logarithmic width  $d \ln k = 0.5$ , and 1000 hrs of integration time (corresponding approximately to the available time within one year of operation). We adjust the noise in  $\Delta_{21}$  using its inverse square-root dependences on the bandwidth and the  $k$ -bin width, and inverse dependence on the integration time (Morales 2005). We use logarithmically spaced bins in both  $k$  and  $1+z$ , and wish to cover a broad redshift range. However, only 32 MHz intervals of data can be computationally handled at a time by the MWA (Lidz et al. 2008), so in order to avoid paying the penalty for reducing the integration time in each frequency interval, we instead reduce the bandwidth around each central redshift by a constant factor that makes the sum of all the bandwidths equal to 32 MHz. We also account approximately for the effect of foregrounds by assuming that the power spectrum cannot be measured below  $k \approx 0.1 h/\text{Mpc}$ , since foreground removal based on the smooth spectrum of the foregrounds will also remove large-scale power in the signal.

Figure 6 shows an example of the expected observa-

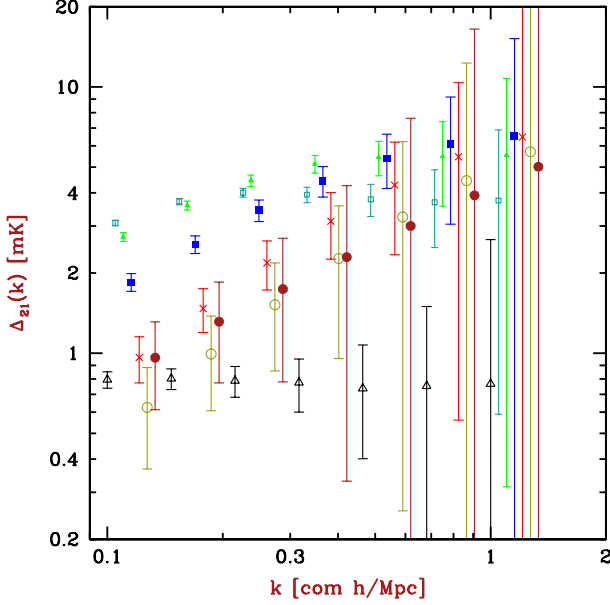


**Figure 6.** Example of predicted values and expected observational errors of the 21-cm power spectrum, for a year of observations with the MWA assuming a reionization model that sets  $V_c = 35$  km/s with a constant efficiency fixed to yield  $\bar{x}^i = 98\%$  at  $z = 6.5$ . The power spectrum is shown at 7 redshifts (out of the actual total number of 19):  $z = 6.5$  ( $\bar{x}^i = 98\%$ , open triangles),  $z = 7.2$  ( $\bar{x}^i = 67\%$ , open squares),  $z = 8.0$  ( $\bar{x}^i = 44\%$ , closed triangles),  $z = 8.9$  ( $\bar{x}^i = 27\%$ , closed squares),  $z = 9.8$  ( $\bar{x}^i = 15\%$ ,  $\times$  symbols),  $z = 10.9$  ( $\bar{x}^i = 7.9\%$ , open circles), and  $z = 12$  ( $\bar{x}^i = 3.7\%$ , closed circles). The same 7  $k$  values are assumed at each redshift, but points at higher  $z$ 's are successively offset to the right for clarity.

tional errors in the 21-cm power spectrum, assuming a year of observations with the MWA, at 19 central redshifts between  $z = 6.5$  and 12 (logarithmically spaced in  $1 + z$ ) and at 7 logarithmically spaced central  $k$  values between 0.1 and  $1h/\text{Mpc}$ . The absolute errors are large at high redshift, mainly because of the increase of the sky temperature which is dominated by the Galactic synchrotron emission. Towards the end of reionization, the relative errors increase as the expected signal itself decreases. Also, the error at a given redshift increases roughly linearly with  $k$  (but faster at the high- $k$  end) when plotted in terms of  $\Delta_{21}(k)$ .

### 3.2 Maximum likelihood fits

In this section we arrive at our goal of obtaining quantitative estimates of the expected uncertainties from modeling the 21-cm power spectrum as observed in one year of operation of the MWA. We consider the errors both in reconstructing the reionization history and the properties of the ionizing sources. We derive the errors from the covariance matrix that depends on the second derivatives of  $\chi^2$  near its minimum; these errors should be accurate as long as they are small, which is the case over most of the parameter space considered below. We consider models that specify the galactic halo population using between 2 and 6 free parameters, as described in section 2.1. Unless otherwise indicated, our input models assume constant values for  $V_c$  and  $\zeta$  (corre-

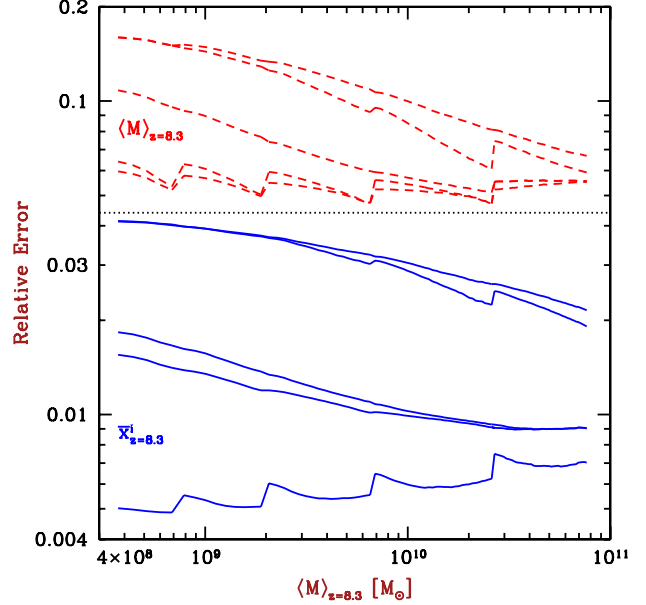


**Figure 7.** Expected errors at the midpoint of reionization (fixed to occur at  $z = 8.3$ ) from fitting models to 21-cm data. We consider models with 2–6 free parameters (bottom to top in each set of curves). A horizontal dashed line separates the two areas of the plot that show the relative errors in the intensity-weighted mean halo mass (top) and cosmic mean ionized fraction (bottom).

sponding to the 2-parameter model) even when we allow additional parameters to vary when fitting to the resulting power spectrum.

Figure 7 shows the expected relative errors in measuring at  $z = 8.3$  the two main quantities of interest, the cosmic mean (mass-weighted) ionization fraction  $\bar{x}^i$  and the mean mass  $\langle M \rangle$  of the halos that contain the ionizing sources (weighted by ionization intensity, which we approximate accurately as weighting by halo mass times number density). The expected errors in these quantities are shown as a function of  $\langle M \rangle$  of the input model, in which the assumed efficiency is set in each case to make  $\bar{x}^i = 50\%$  at  $z = 8.3$  (which is one of the 19 measured redshifts).

The halo mass range shown in Figure 7 (as well as 8) corresponds to the range  $V_c = 16.5 - 125$  km/s, where the lowest value corresponds to the minimum halo mass in which virialized gas can cool via radiative transitions in atomic hydrogen and helium (which requires a virial temperature of  $\sim 10^4$  K). For a fixed number of parameters, the errors tend to decrease with increasing halo mass, since if rare, massive halos drive reionization then the halo bias is larger, increasing the large-scale ionization fluctuations and making the power spectrum more easily observable (as shown in the previous subsection). The curves, however, sometimes show a jump in the error value as  $\langle M \rangle$  is increased past certain values. Each of these values corresponds to another one of the (fixed) measured redshifts going below the end of reionization (since the redshift  $z_{\text{rei}}$  at the end of reionization becomes closer to the midpoint,  $z = 8.3$ , as  $\langle M \rangle$  is increased). Measurements at  $z < z_{\text{rei}}$  do not constrain the parameters, and this reduces the constraints on the measured parameters even at  $z > z_{\text{rei}}$ ; this effect is small for the

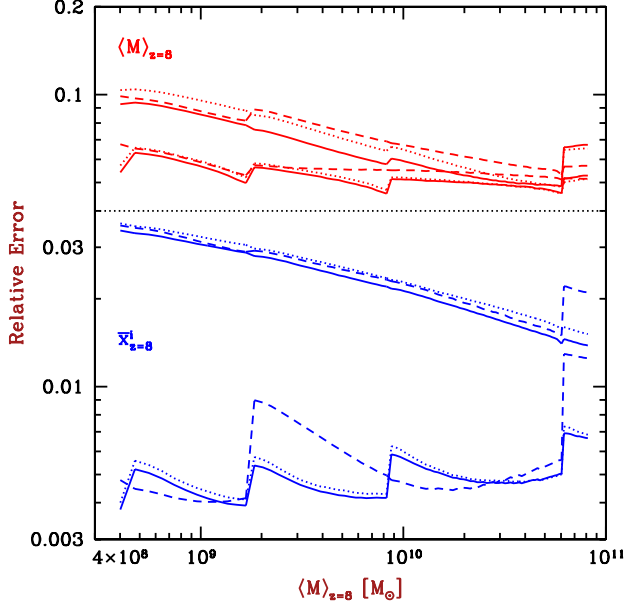


**Figure 8.** Expected errors at  $\bar{x}^i = 60\%$  (fixed to occur at  $z = 8$ ) from fitting models to 21-cm data. We consider observations at 19 redshifts and 7 wavenumbers (our standard case, solid curves), 19 redshifts and 4 wavenumbers (dotted curves), or 10 redshifts and 7 wavenumbers (dashed curves), where in all cases the assumed observing time and the total  $z$  and  $k$  ranges remain the same, and the  $z$  and  $k$  bins are logarithmically spaced. We only show models with either 2 or 6 parameters, where the higher curve of each pair corresponds to having 6 parameters. A horizontal dashed line separates the two areas of the plot that show the relative errors in  $\langle M \rangle$  (top) and  $\bar{x}^i$  (bottom).

more flexible models, in which the parameters at different redshifts are more independent of each other.

Figure 8 shows how the expected errors depend on the number of bins used in redshift and in wavenumber. We consider a slightly more advanced stage of reionization,  $\bar{x}^i = 60\%$ , fixed to occur at  $z = 8$  (which is one of the measured redshifts in both of the cases that we consider here for redshift bins). For our standard case of observations at 19 redshifts and 7 wavenumbers, the errors are similar to those in Figure 7, except that the error in  $\langle M \rangle$  is less dependent on the number of model parameters, i.e.,  $\langle M \rangle$  is measured at  $\bar{x}^i = 60\%$  better than at  $\bar{x}^i = 50\%$  for the 6-parameter model. Reducing the number of  $k$  bins from 7 to 4 has a rather minor effect on the errors, qualitatively consistent with Lidz et al. (2008) who argued that the MWA can essentially only measure the amplitude and slope of the 21-cm power spectrum at each redshift. Reducing the number of redshifts from 19 to 10 can have a bigger effect, producing larger jumps in the error near some values of  $\langle M \rangle$ . Clearly, it is best to divide the available 32 MHz total bandwidth into a large number of redshift bins. Note that we make a slight approximation in our calculations in that we compare the data and the models at the center of the  $z$  and  $k$  bins, while a more exact comparison would average the theoretical signal over the  $z$  and  $k$  range within each bin.

The complete result that we can derive from our analysis is the expected error in reconstructing the history of reionization and of the ionizing sources within the observed

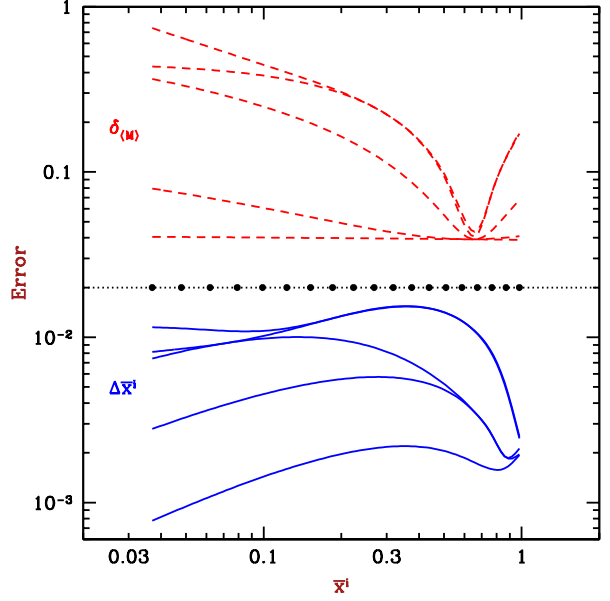


**Figure 9.** Expected errors throughout reionization, from fitting models to 21-cm data. We consider models with 2–6 parameters (bottom to top in each set of curves). The input model sets  $\bar{x}^i = 98\%$  at  $z = 6.5$  with  $V_c = 35$  km/s. A horizontal dashed line separates the two areas of the plot that show the relative error in the intensity-weighted mean halo mass (top) and the *absolute* error in the ionized fraction (bottom). Dots on this line show the values of  $\bar{x}^i$  corresponding to the 19 observed redshifts.

redshift range of  $z = 6.5 - 12$ . This result is shown in Figures 9 and 10, for halos with minimum  $V_c = 35$  and 100 km/s, respectively. While we again show the relative error  $\delta_{\langle M \rangle}$ , we now show the *absolute* error  $\Delta \bar{x}^i$  because this quantity varies far less during reionization than does  $\delta_{\bar{x}^i}$ . The relative error  $\delta_{\bar{x}^i}$  increases strongly with redshift, and becomes rather large at early times when  $\bar{x}^i$  is itself small (e.g., for  $V_c = 35$  km/s and the 6-parameter model,  $\delta_{\bar{x}^i} \sim 0.3$  when  $\bar{x}^i = 0.04$ ). Note that the same redshift range,  $z = 6.5-12$ , corresponds to a substantially wider portion of reionization (in terms of the range of  $\bar{x}^i$ ) for the more massive galactic halos.

The figures show that in general, a model with a small number of parameters has errors that are relatively uniform throughout reionization, since in such a restricted model the values of  $\bar{x}^i$  and  $\langle M \rangle$  are strongly coupled throughout reionization, producing similar, strongly correlated errors at all redshifts. As the number of parameters allowed to vary freely is increased, the expected errors obviously increase as well.

However, there are two special quantities that are well measured regardless of the number of model parameters: the mean halo mass at  $\bar{x}^i \sim 65\%$ , and  $\bar{x}^i$  itself near the very end of reionization. The measurement of  $\langle M \rangle$  results mainly from the strong dependence of the large-scale 21-cm power spectrum on halo bias near the mid-point of reionization. The large-scale power at this stage is the best-measured region out of all of reionization, in terms of small relative measurement errors in  $\Delta_{21}(k)$  (as illustrated in Figure 6). The measurement errors, which increase rapidly with redshift due to the frequency dependence of the galactic fore-

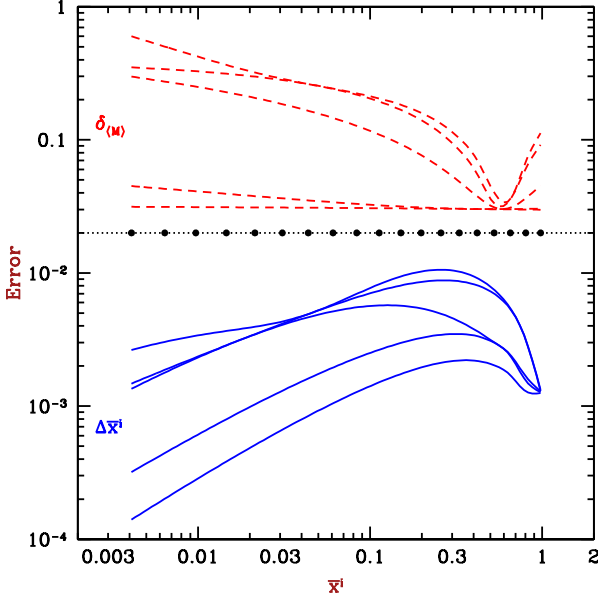


**Figure 10.** Same as Figure 9, except that the input model sets  $\bar{x}^i = 98\%$  at  $z = 6.5$  with  $V_c = 100$  km/s.

ground, push the best-measured points to later times, resulting in  $\langle M \rangle$  being best measured at around the 2/3 mark of cosmic reionization. Separately, the evolution of  $\bar{x}^i$  at the very end of cosmic reionization is measured accurately as well, since the disappearance of the last remaining pockets of neutral low-density gas causes a rapid decline with redshift in the 21-cm power spectrum, making it highly sensitive to small changes in  $\bar{x}^i$  at a given redshift. This decline is well measured because of the low thermal noise within the corresponding, relatively low, redshifts (as also illustrated in Figure 6).

We have thus far tested only input models with constant values of  $V_c$  and  $\zeta$  throughout reionization, but we now consider also an example of a model with redshift-dependent parameters; in this model, which is loosely motivated by feedback models, the minimum halo  $V_c$  increases with time (perhaps due to photo-heating feedback), decreasing the number of halos, but this is counter-acted by an increasing ionizing efficiency with time (perhaps due to supernova feedback being less effective in the massive halos that dominate at later times). Specifically, given a redshift at which reionization is nearly complete (defined here as having  $\bar{x}^i = 98\%$ ), we let  $V_c$  decrease linearly with redshift, going from the atomic-cooling value of 16.5 km/s at  $z = 12$  to 35 km/s when  $\bar{x}^i = 98\%$ . Meanwhile,  $\zeta$  is assumed to be proportional to  $V_c^2$ , which implies in this model a quadratic dependence on redshift.

Figure 11 shows our results of fitting the 6-parameter model to eight different input models. We consider low-mass halos corresponding to the minimum mass for atomic cooling ( $V_c = 16.5$  km/s), intermediate-mass halos ( $V_c = 35$  km/s), high-mass ones ( $V_c = 100$  km/s), and the feedback-inspired model, each with reionization ending at low redshift ( $\bar{x}^i = 98\%$  at  $z = 6.5$ ) or at a relatively high redshift ( $\bar{x}^i = 98\%$  at  $z = 7.8$ ). As already noted, the models with high-mass halos allow a higher-precision reconstruction, especially early on

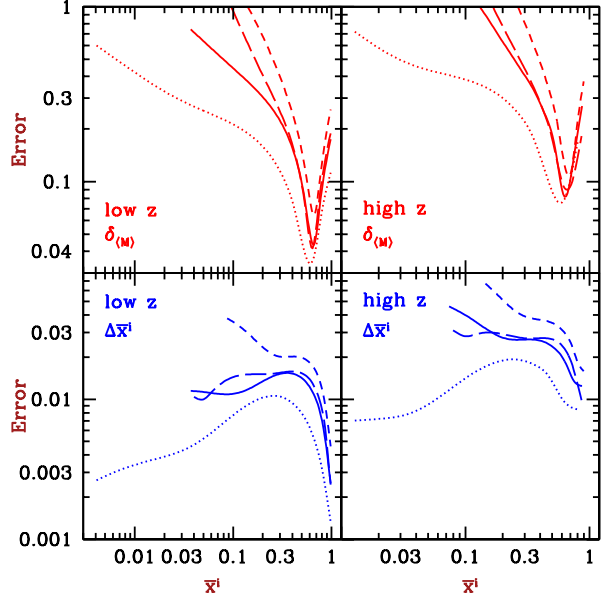


**Figure 11.** Expected errors throughout reionization, from fitting our full 6-parameter model to 21-cm data. We consider input models that set  $\bar{x}^i = 98\%$  at redshift 6.5 (low  $z$ : left panels) or at  $z = 7.8$  (high  $z$ : right panels). We consider galactic halos with minimum  $V_c = 16.5$  km/s (short-dashed curves), 35 km/s (solid curves), 100 km/s (dotted curves), or our feedback-inspired model (long-dashed curves). For each model we show the relative error in the intensity-weighted mean halo mass (top panels) and the absolute error in the ionized fraction (bottom panels).

in reionization (i.e., at low  $\bar{x}^i$ ), but with smaller errors even at the late stages, by a factor of up to 2 though usually less, especially for  $\langle M \rangle$ . Higher-redshift reionization leads predictably to somewhat larger errors, typically by a factor of  $\sim 2$  as expected from the increase of the sky brightness from redshift 6.5 to 7.8. The results shown at the very end of reionization are affected by the redshift binning: while in the low-redshift models, the lowest-redshift bin ( $z = 6.5$ ) falls right at the end of reionization ( $\bar{x}^i = 98\%$ ), the high-redshift models are an example where the lowest-redshift bin that is still during reionization falls somewhat earlier ( $z = 8$ , which corresponds to  $\bar{x}^i = 81\%$  for  $V_c = 100$  km/s and  $\bar{x}^i \sim 90\%$  for the other models).

The feedback-inspired model, which is identical to the constant  $V_c = 35$  km/s model at the end of reionization but has lower  $V_c$  and higher  $\zeta$  values earlier on, gives errors that are generally fairly close to those of the  $V_c = 35$  km/s model. This indicates that there is some correlation of the constraints at different redshifts through the model parameters, which are limited to six (a small number compared to the total number of measured data points); the constraints on the model parameters are dominated by the central and late stages of reionization, where the observational errors are small (and where the feedback-inspired model is nearly identical to the  $V_c = 35$  km/s model).

The conclusions from these figures are rather positive in terms of the prospects for learning about high-redshift astrophysics from the upcoming 21-cm experiments. On the one hand, our lack of independent knowledge of the prop-

erties of the ionizing sources has a substantial effect on our expected ability to reconstruct both the reionization history and the properties of the sources; in particular, allowing a model with 6 free parameters raises the errors by up to an order of magnitude compared to fitting with a model restricted to just 2 parameters. On the other hand, even with a 6-parameter model that allows for a fairly large parameter space of galaxy properties, the one-year MWA observations allow a rather impressive reconstruction of reionization. Even the worst case in Figure 11, of high-redshift reionization and low-mass atomic-cooling halos, yields relative errors of  $\sim 10\%$  in  $\langle M \rangle$  when  $\bar{x}^i \sim 2/3$ , and  $2\%$  in  $\bar{x}^i$  at the end of reionization. In the best case of low-redshift reionization (including an observed redshift bin centered at the 98% mark of cosmic reionization) together with high-mass source halos, these relative errors drop to  $4\%$  and  $0.2\%$ , respectively. The errors in  $\langle M \rangle$  and  $\bar{x}^i$  are also remarkably low throughout the central stage of reionization.

#### 4 CONCLUSIONS

We have used the most realistic fully analytical model available for the 21-cm power spectrum (Barkana 2007) to fit models of the galaxy population during reionization to simulated 21-cm power spectrum observations. The model assumes at each redshift a fixed ionizing efficiency  $\zeta$  and a minimum halo circular velocity  $V_c$  for galactic halos. Allowing each of these quantities to vary linearly or quadratically with redshift yields reionization models with up to 6 parameters, which we allow to vary freely without any restrictions based on specific models of feedback.

Before proceeding, we compared the analytical model of Barkana (2007) to the results of three different groups that have run N-body simulations, processed the outputs with radiative transfer, and calculated the 21-cm power spectrum at various redshifts during the reionization epoch. The simulations are all in reasonable agreement with the analytical model (Figures 1–3), with typical differences in  $\Delta_{21}$  in the range  $\sim 10 - 30\%$ . While the analytical model makes various simplifying assumptions, the simulations are also limited by box size and radiative transfer resolution. The analytical model generally captures the evolution of the 21-cm power spectrum during reionization as seen in the simulations, but a more precise comparison must await a demonstration that the simulations have numerically converged and are consistent with each other.

As discussed in earlier sections, the model used here should not be considered the ultimate model to use in fitting the 21-cm power spectrum during reionization, but as an important step towards a final model to be constructed using guidance from numerical simulations. The main qualitative limitation of the model used here is that while it allows a redshift dependence in the properties of galactic halos, the parameters are limited to being spatially uniform at each redshift. A more realistic model would add the possibility of spatially inhomogeneous (in particular, density-dependent) feedback. However, we note that any such extension, which will likely add substantial complexity to the model, must still allow a relatively quick calculation of the 21-cm power spectrum in order to permit a maximum likelihood analysis. It will also be important to keep the model flexible

without relying too heavily on results of particular models or simulations, where feedback processes can only be included with limited and approximate methods. We note that McQuinn et al. (2007) considered the effect of minihalos and Lyman-limit systems in limiting the mean free paths of ionizing photons, and showed that their effect on the 21-cm power spectrum at a given  $\bar{x}^i$  is rather small and is much less significant than the effect of the halo mass of the ionizing sources.

The maximum likelihood fitting yields good grounds for optimism. While our ignorance regarding the properties of the ionizing sources has a substantial effect on the expected errors, we still conclude that the expected measurements of the 21-cm power spectrum will enable us to reconstruct both the reionization history and the properties of the sources. In particular, even with a 6-parameter model that allows for a fairly large parameter space of galaxy properties, the one-year MWA observations allow a remarkably precise reconstruction of reionization.

As a specific example of the expected errors, if reionization ends at  $z = 6.5$  and is dominated by intermediate-mass halos (minimum halo circular velocity  $V_c = 35$  km/s, corresponding to a mean halo mass of ionizing sources  $\langle M \rangle \sim 3 \times 10^9 M_\odot$  at the midpoint of reionization), then the cosmic mean ionized fraction can be measured to  $0.3\%$  accuracy at the very end of reionization, to a relative accuracy of a few percent around the mid-point of reionization, and better than  $10\%$  as early as a cosmic mean ionized fraction of  $\bar{x}^i = 10\%$ . Also, the mean halo mass of the ionizing sources can be measured in this case to  $5\%$  accuracy when reionization is  $2/3$  of the way through, and to  $20\%$  accuracy throughout the last  $2/3$  of reionization (i.e., when  $\bar{x}^i$  between  $1/3$  and  $1$ ). The errors in general increase with the redshift at which reionization ends, and decrease with the halo mass of the dominant ionizing sources.

The best-measured point of reionization is around the  $2/3$  mark in terms of precision in  $\langle M \rangle$ , and near the very end of reionization in terms of precision in  $\bar{x}^i$ . The errors, though, are fairly small in the central and late stages of reionization for all the models that we have examined (see especially Figure 11), which include halos that range from the atomic-cooling minimum ( $V_c = 16.5$  km/s,  $\langle M \rangle \sim 4 \times 10^8 M_\odot$ ) to 200 times more massive halos ( $V_c = 125$  km/s,  $\langle M \rangle \sim 8 \times 10^{10} M_\odot$ ), examined for reionization that ends at  $z \sim 6.5$  or  $z \sim 8$ . We thus conclude that if the upcoming 21-cm experiments, after foregrounds are removed and instrumental systematics are dealt with, reach anywhere near their expected sensitivity, then they will allow us to study high-redshift astrophysics in unprecedented detail.

#### ACKNOWLEDGMENTS

The author is grateful for support from the ICRR in Tokyo, Japan, the Moore Distinguished Scholar program at Caltech, and the John Simon Guggenheim Memorial Foundation, as well as Israel Science Foundation grant 629/05.

#### REFERENCES

Barkana R., 2007, MNRAS, 376, 1784

- Barkana R., Loeb A., 2004, ApJ, 609, 474  
 Barkana R., Loeb A., 2008, MNRAS, 384, 1069  
 Bond J. R., Cole S., Efstathiou G., Kaiser N., 1991, ApJ, 379, 440  
 Dunkley J., et al., 2008, ApJS, submitted (arXiv:0803.0586)  
 Fan X., Carilli C. L., Keating B., 2006, ARAA, 44, 415  
 Furlanetto S. R., Zaldarriaga M., Hernquist L., 2004, ApJ, 613, 1  
 Iliev I. T., Mellema G., Pen U.-L., Bond J. R., Shapiro P. R. 2008, MNRAS, 384, 863  
 Komatsu E., et al., 2008, ApJS, submitted (arXiv:0803.0547)  
 Lidz A., Zahn O., McQuinn M., Zaldarriaga M., Hernquist L., 2008, ApJ, submitted (arXiv:0711.4373)  
 Loeb A., Zaldarriaga M. 2004, PRL, 92, 211301  
 Madau, P., Meiksin, A., & Rees, M. J. 1997, ApJ, 475, 429  
 McQuinn M., Zahn O., Zaldarriaga M., Hernquist L., Furlanetto S. R., 2006, ApJ, 653, 815  
 McQuinn M., Lidz A., Zahn O., Dutta S., Hernquist L., Zaldarriaga M., 2007, MNRAS, 377, 1043  
 Mesinger A., & Furlanetto S. 2007, ApJ, 669, 663  
 Morales M. F. 2005, ApJ, 619, 678  
 Press W. H., Schechter P. 1974, ApJ, 187, 425  
 Santos M. G., Amblard A., Pritchard J., Trac H., Cen R., Cooray A. 2008, submitted (arXiv:0708.2424)  
 Scannapieco E., Barkana R., 2002, ApJ, 571, 585  
 Seljak U., Zaldarriaga M. 1996, ApJ, 469, 437  
 Sheth, R. K., & Tormen, G. 1999, MNRAS, 308, 119  
 Zahn O., Lidz A., McQuinn M., Dutta S., Hernquist L., Zaldarriaga M., Furlanetto S. R., 2007, ApJ, 654, 12